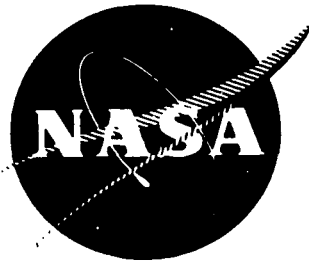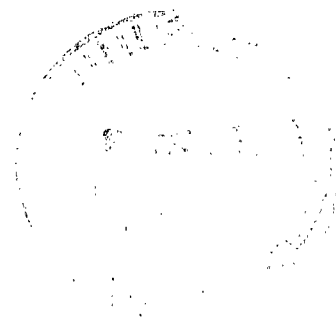NASA CR-135318

CHARGE-EXCHANGE PLASMA

GENERATED BY AN ION THRUSTER

PREPARED FOR

LEWIS RESEARCH CENTER

NATIONAL AERONAUTICS AND SPACE ADMINISTRATION

GRANT NSG 3038

Annual Report

December 1977

Harold R. Kaufman

Department of Mechanical Engineering

Colorado State University

Fort Collins, Colorado

1. Report No. NASA CR-135318	2. Government Accession No.	3. Recipient's Catalog No.
4. Title and Subtitle CHARGE-EXCHANGE PLASMA GENERATED BY AN ION THRUSTER (U)		5. Report Date December 1977
		6. Performing Organization Code
7. Author(s) Harold R. Kaufman		8. Performing Organization Report No.
		10. Work Unit No.
9. Performing Organization Name and Address Department of Mechanical Engineering Colorado State University Fort Collins, Colorado 80523		11. Contract or Grant No. NSG 3038
		13. Type of Report and Period Covered Contractor Report Nov. 1, 1976 - Dec. 31, 1977
12. Sponsoring Agency Name and Address National Aeronautics and Space Administration Washington, D.C. 20546		14. Sponsoring Agency Code

15. Supplementary Notes

Grant Manager, Stanley Domitz
NASA Lewis Research Center
Cleveland, OH 44135

16. Abstract

The charge-exchange plasma generated by an ion thruster has been investigated experimentally using both 5-cm and 15-cm thrusters. The results of this investigation are shown for wide ranges of radial distance from the thruster and angle from the beam direction. Considerations of test environment, as well as distance from the thruster, indicate that a valid simulation of a thruster on a spacecraft was obtained. A calculation procedure and a sample calculation of charge-exchange plasma density and saturation electron current density are included.

17. Key Words (Suggested by Author(s)) Electrostatic thruster, Plasma physics, Electric propulsion	18. Distribution Statement Unclassified - Unlimited		
19. Security Classif. (of this report) Unclassified	20. Security Classif. (of this page) Unclassified	21. No. of Pages	22. Price*

i

TABLE OF CONTENTS

INTRODUCTION

A charge-exchange process occurs between energetic beam ions from an ion thruster and the escaping neutrals. As the result of this process, slow ions are generated. These slow ions, together with electrons that escape from the ion beam, form the charge-exchange plasma that surrounds an ion thruster. The presence of this charge-exchange plasma explains the observation of large electron currents to positive surfaces near thrusters.[1] Without the presence of ions to neutralize the electron space charge, these currents would be much smaller.[2] The characteristics of this charge-exchange plasma are important for space missions where ion thrusters are used with high voltage solar arrays. The characteristics may also be of interest in predicting the environmental effects on scientific instruments that are used on an electrically propelled spacecraft.

The first support period of this Grant was directed at a preliminary study of the charge-exchange plasma.[3] A model was developed that gave reasonable agreement with the experimental measurements obtained in this study. The next support period of this Grant was directed primarily at the collection or direction control of the charge-exchange ions.[4] Several cones, both screened and solid, were placed on the thruster around the ion beam. Even with the use of bias voltages, these cones did little more than move the effective source of charge-exchange ions in the downstream direction. Some estimates of electron collection were also made for a positive high voltage solar array on a spacecraft. Using an unprotected array for the beam power of an ion thruster, or thrusters, the collected electron current would be less than 10 percent of the array current below about 300 volts. Coverings

of insulation might permit substantially higher voltages.

The present and final support period of this Grant was directed
at a wider range of experimental parameters. This wider range should
give better experimental justification for spacecraft calculations.

The results of all support periods are summarized in this final
report with regard to charge-exchange plasma propagation. For example,
equations for electron density and electron saturation current density
were obtained from the isotropic propagation model. These equations
are the basis for scaling plasma propagation, and are therefore re-
peated. The derivationsof these equations, however, are not repeated.
To further aid in calculations of charge-exchange plasma propagation,
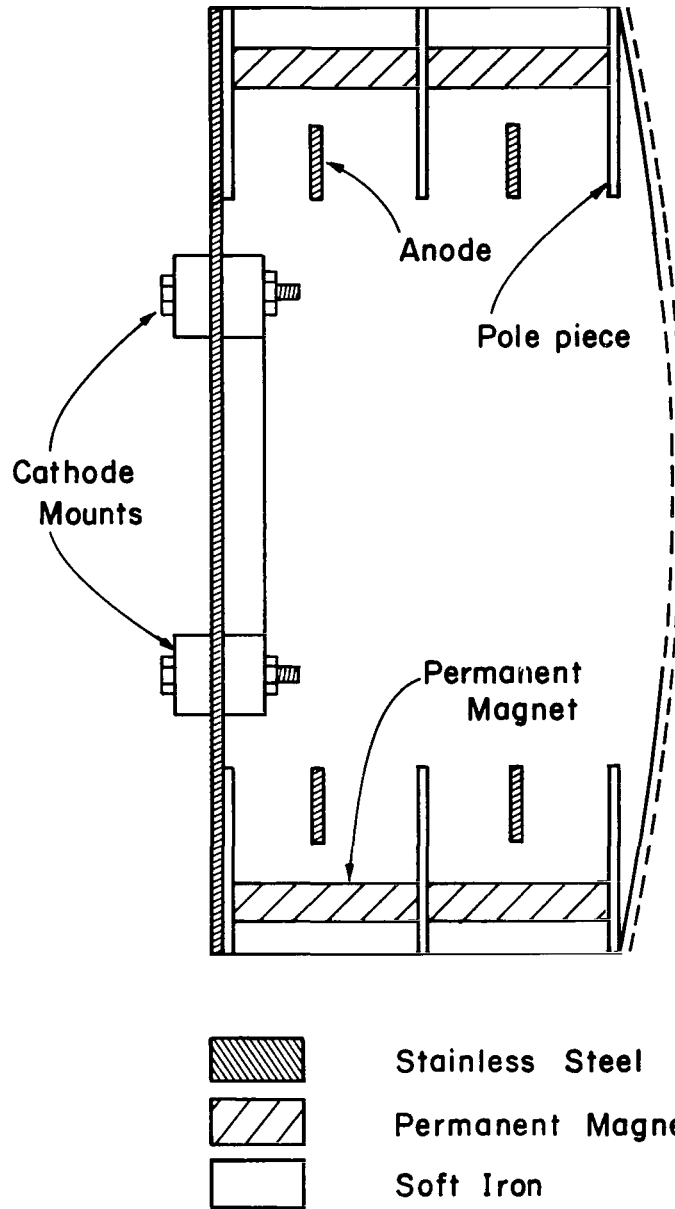a procedure is detailed in a separate section.

APPARATUS AND PROCEDURE

The vacuum facility used was the 1.2-m diameter, 4.6-m long chamber at the Engineering Research Center of Colorado State University. An 0.8-m diffusion pump maintained pressures in the mid-10^{-6} Torr range during thruster operation. A liquid-nitrogen cooled liner helped maintain this pressure by condensing the mercury propellant.

Some data from earlier support periods of this Grant are included in this report. These earlier data were obtained with a modified SERT-II thruster. The modification consisted of dished molybdenum grids that permitted higher beam currents than the original flat grids.

Data during the last support period of this Grant were obtained with a 5-cm multipole thruster designed and built for this investigation. This multipole thruster (see Fig. 1) had a discharge chamber 7.6 cm in diameter and a surrounding screened enclosure that was 17.8 cm in diameter. Tungsten wire, 0.25 mm in diameter, was used for both the main and neutralizer cathodes.

The Langmuir probes used in the charge-exchange plasma survey were of a guarded construction, as indicated in Fig. 2. Surveys with this probe design extended from 26 cm upstream of the SERT-II accelerator grid to 49 cm downstream. Some of these earlier data are included herein. For the last Grant support period with the 5-cm thruster, the survey planes (I-VI) are indicated in Fig. 3. Langmuir probe measurements were made at several radii (from the thruster axis) in each of these planes. For survey planes I-III, measurements were made at radii of 12.3, 17.3, 18.7, 22.2, 24.0, 27.1, 29.6, 32.1, 35.4, and 41.3 cm. For planes IV-VI the radii were 10.9, 15.2, 15.5, 19.3, 20.7, 23.6, 26.1, 27.9, 31.6, and 37.1 cm. This survey included more

Anode

Pole piece

Cathode
Mounts

Permanent
Magnet

Stainless Steel

Permanent Magnet

Soft Iron

(a) Sketch of cross section. Note screen is masked to 5-cm diameter.

Fig. 1 Multipole thruster used in investigation
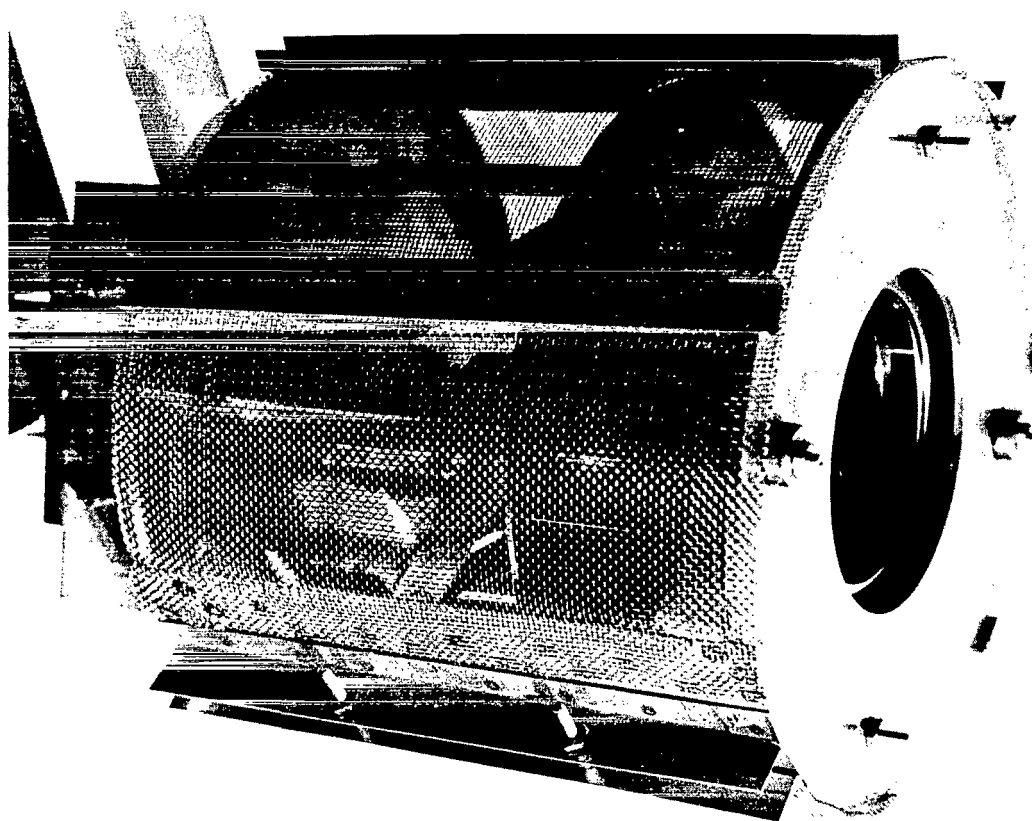
(b) Photograph of completed thruster.
Accelerator system removed to show
pole piece and anode construction.

Fig. 1 Concluded.

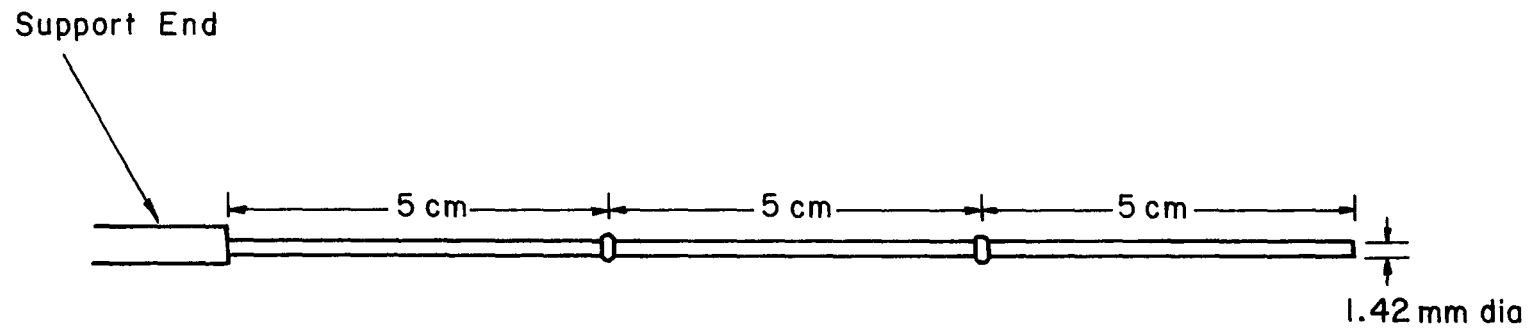Support End

5 cm | 5 cm | 5 cm

1.42 mm dia

Fig. 2 Guarded Langmuir probe used in survey of charge-exchange plasma.
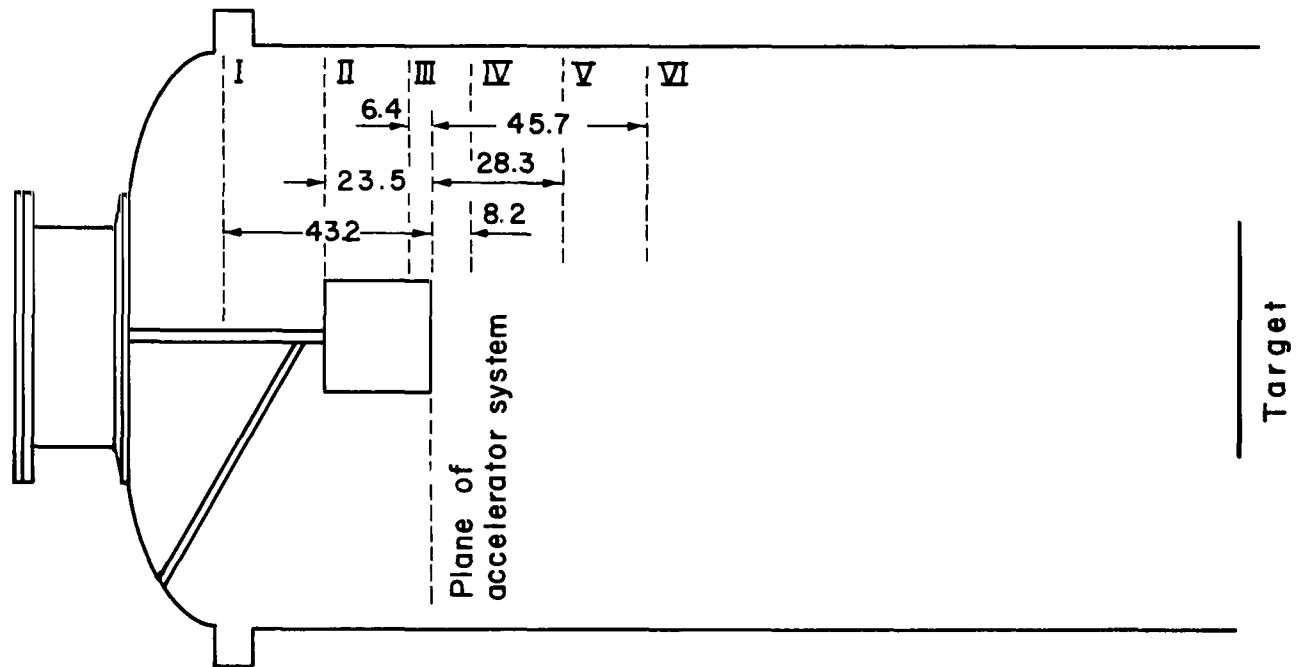
Fig. 3   Locations of survey planes.

locations than the SERT-II survey, as well as extending farther up-stream of the thruster. A thick sheath procedure was required to reduce the Langmuir probe data because the probe diameter was generally much smaller than the Debye length. The procedure used is described by Isaacson[5] and is based on the theory and methods of Chen.[6]

Two additional probes were used during the 6-cm tests. These were the guarded planar probe (see Fig. 4.) and the "pin-hole" probe (see Fig. 5.). The pin-hole probe, as indicated in Fig. 5., used both a plain polyimide surface (Kapton, about 0.13 mm thick) and grounded conducting meshes attached to that surface. Both meshes were constructed of about 1 mm wide copper strips. The conductor behind the pin hole was stainless steel. Although this conductor was in close proximity to the polyimide, it was not cemented or glued to the polyimide.

An ion beam target was placed at the middle of the vacuum chamber and electrically isolated from that chamber. All thruster operation was at +1000 and -500V. The 5-cm thruster was operated with a 70 mA-equivalent neutral flow and a 50 mA ion beam.
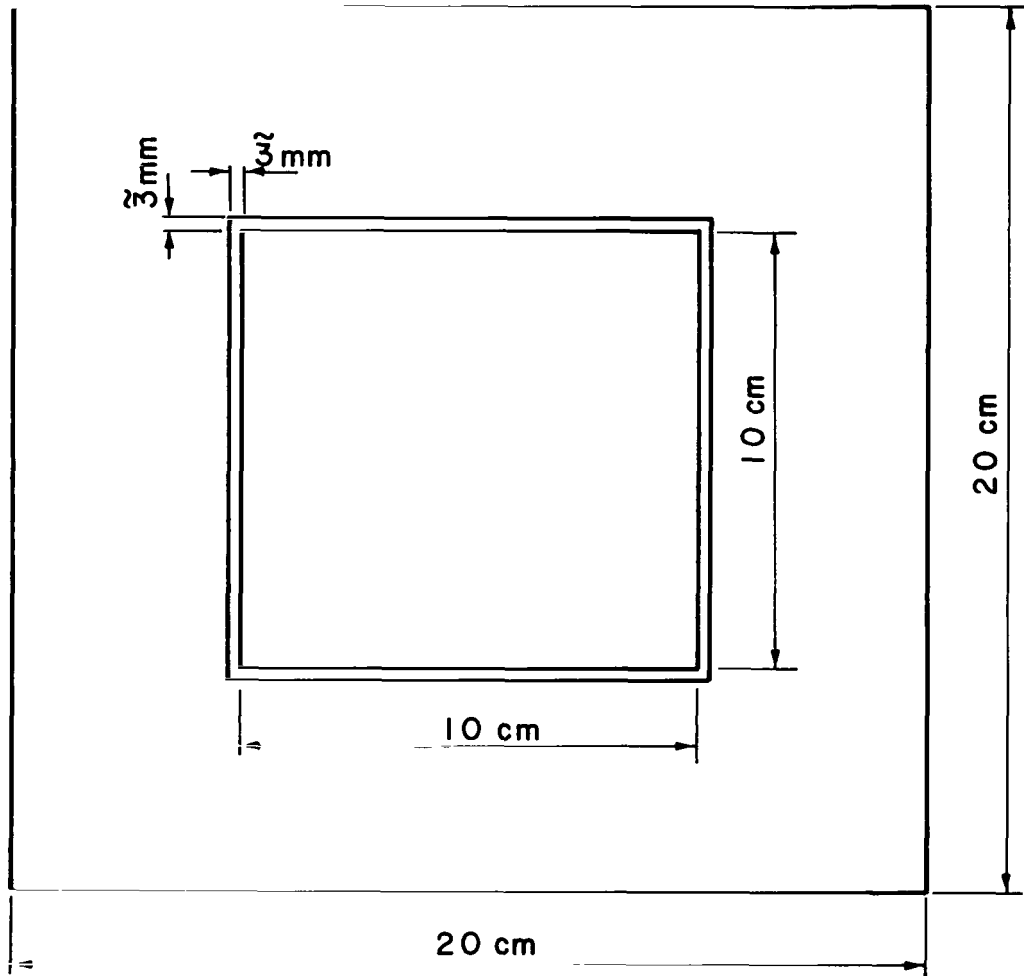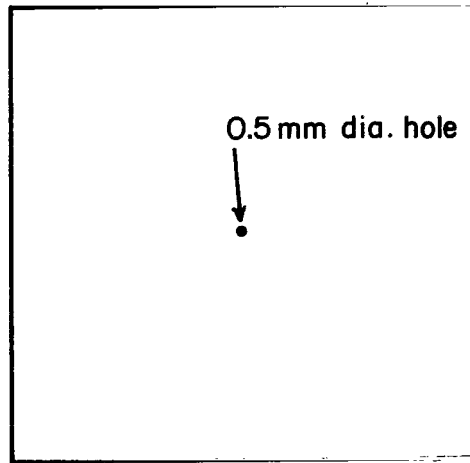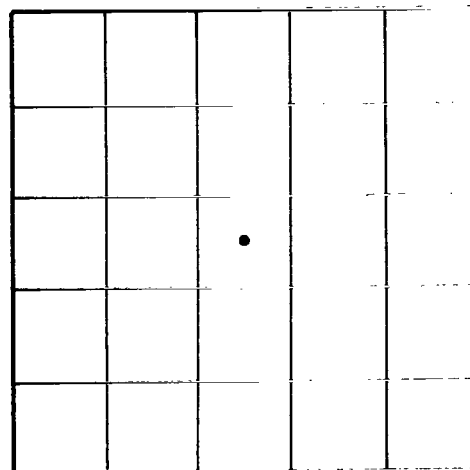
Fig. 4 Guarded planar probe.

0.5 mm dia. hole

(a)   Plain probe, 20 cm square.

(b)   Probe with coarse mesh (~ 4 cm).
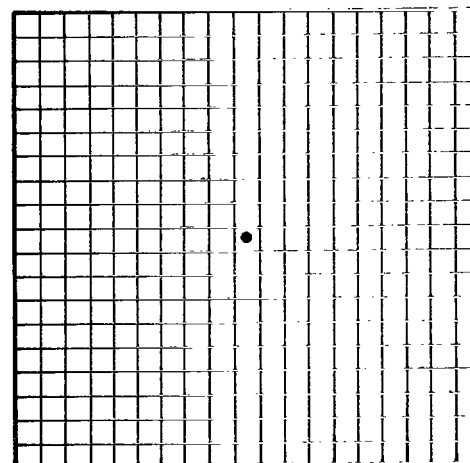
(c)   Probe with fine mesh (~ 1 cm).

Fig. 5 Pin-hole probe configurations tested.

RESULTS AND DISCUSSION

Simulation of Space Environment

The vacuum chamber was negative relative to the charge-exchange plasma to most closely approximate the space environment. In space the charge-exchange ions would continue indefinitely outwards from the thruster. The accompanying electrons would have a drift velocity about equal to the ion velocity, with a much larger random velocity superimposed on this drift velocity. A boundary potential that would collect ions and reflect electrons is thus the best simulation of these conditions in space.

The negative vacuum chamber bias was established by operating the ion-beam target at +60V relative to the chamber. The shielding screen (usually grounded) surrounding the 5 cm thruster was operated at this same potential. Although operation with a positive bias on the target and shielding screen was believed to be the best simulation of space, the results were not found to be critical with respect to this bias. For example, with the target and shielding screen grounded to the vacuum chamber, all electron densities were found to be within a factor of two of the densities obtained with a positive bias. The reason for the lack of any large difference is believed to be the tendency of a plasma to become more positive than the most positive electrode in contact with it. Thus the reflection of electrons and collection of ions would normally be established. Only in very low density regions, where the saturation electron current is small, would a reflection of ions be possible.

Another factor affecting the validity of simulation is the background pressure. Figure 6 shows the effect of changing vacuum chamber pressure by adding additional mercury flow outside the thruster. The lowest pressure shown in Fig. 6. was representative of normal facility operation, while the higher pressures required the additional mercury flow. The electron densities shown in Fig. 6. were from a probe 8.2 cm downstream of the accelerator system and 28 cm radially outwards. Extrapolation to zero pressure gives an indication of the density that might be expected in space. As shown by Fig. 6., this extrapolated density is still about 2/3 of the density at the normal operating pressure. The accuracy of this extrapolation is limited by the estimated ± 50 percent accuracy of the probe density measurements. On the other hand, some of background pressure during normal operation must be due to gases other than mercury. The charge-exchange cross sections of mercury beam ions with these other gases should be much smaller than with mercury. A decrease in pressure due to removal of these other gases should therefore not have a significant effect on the charge-exchange plasma density. In short, most of the charge-exchange plasma around the thruster would still be expected to be present in space.

Survey of Charge-Exchange Plasma

The charge-exchange plasma surrounding the 5-cm ion thruster was surveyed using Langmuir probes. The electron density was the most reproducible plasma property, as well as being the one of most interest. A survey of this density is shown in Fig. 7. This survey is similar to those obtained earlier for the 15-cm thruster, except that a smaller ion-beam diameter was used and the survey extended further upstream
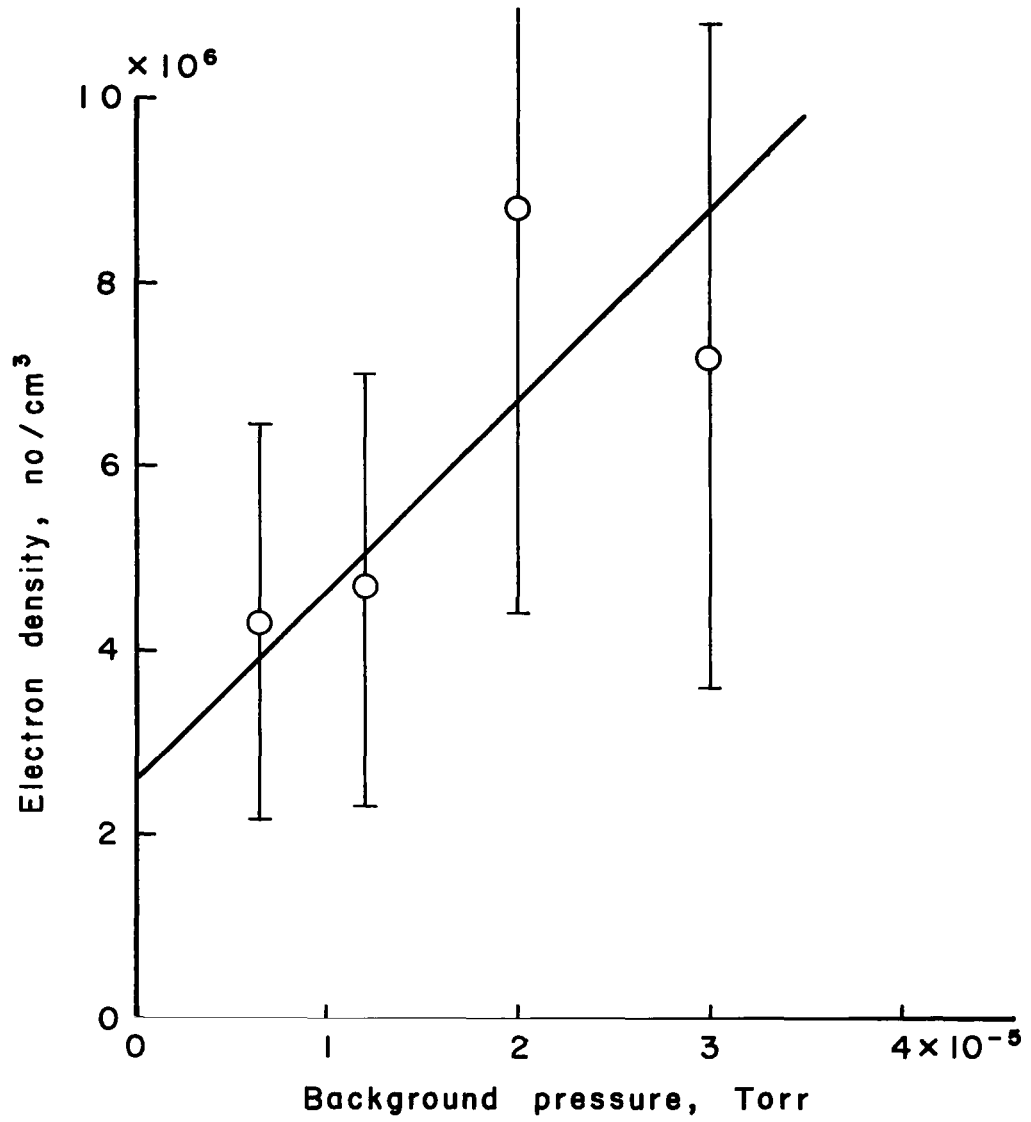
Fig. 6   Variation of electron density with
facility pressure.
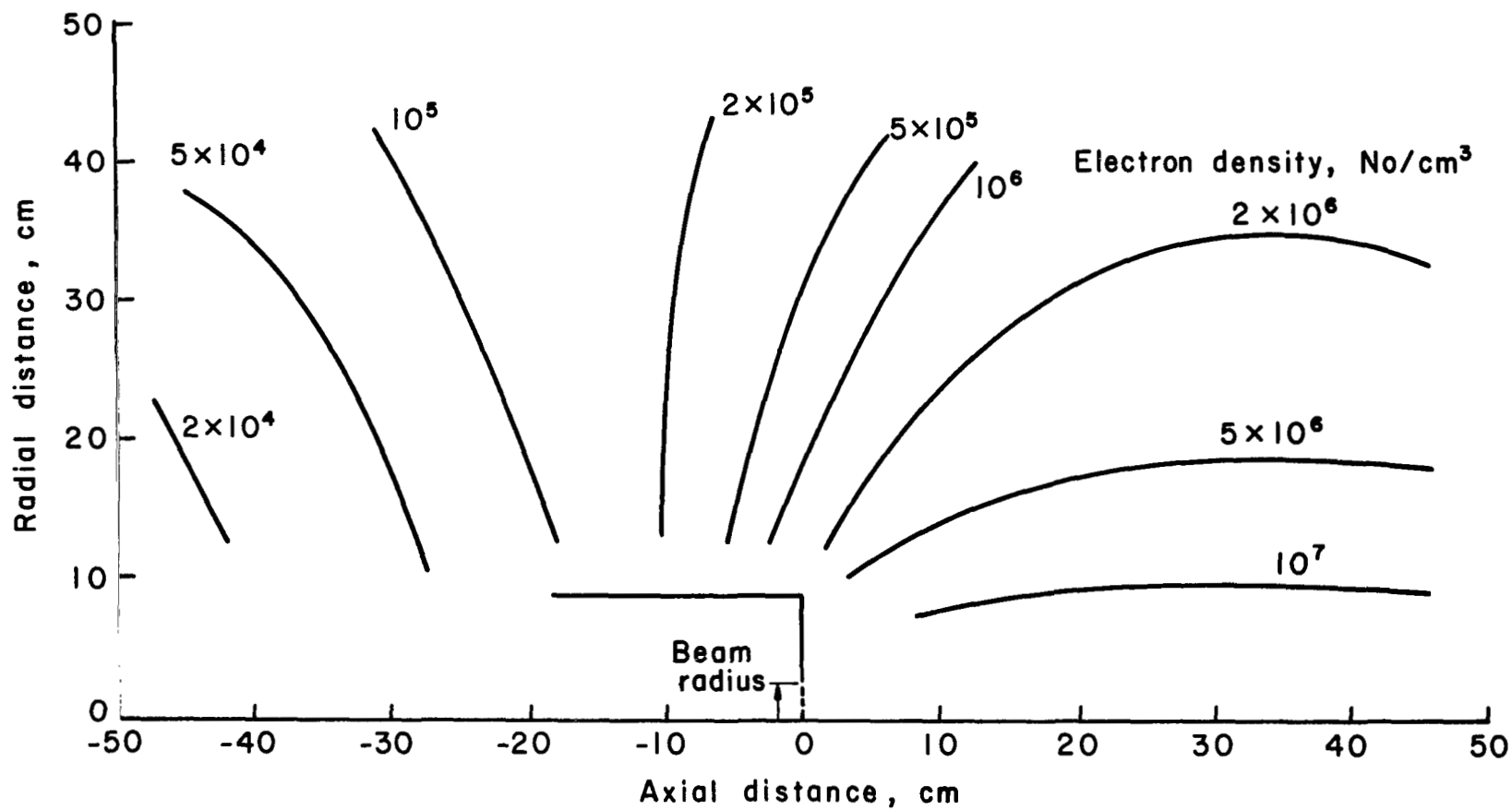
Fig. 7 Survey of electron density with 5-cm thruster.
Beam current, 50 mA; nuetral flow, 70 mA-equivalent.

of the thruster. Both of these changes permitted a more rigorous
evaluation of the transport model and its validity for spacecraft
calculations.

The electron temperature was also obtained from the Langmuir
probes and ranged from about 3 to 4 eV in the charge-exchange region.
This was slightly higher than the 2.5 eV average obtained for the
same region with the 15 cm thruster. A refractory metal neutralizer
was used with the 5-cm thruster, while a plasma bridge neutralizer
was used with the 15-cm thruster. The electron temperature difference
was probably due to the size or neutralizer difference for the two
thrusters.

Radial Variation of Electron Density

The radial variation of electron density is, according to the
isotropic transport model, an inverse-square relationship. In this
model the production of charge-exchange ions is calculated by approxi-
mating the neutral density downstream of the thruster with the known
solution downstream of a circular sharp-edged orifice. For the purpose
of simplifying the calculations and obtaining a conservative answer,
the ion beam was assumed to be concentrated near the axis of the
neutral efflux. With the further assumptions of plasma neutrality
and that the charge-exchange ions leave at Bohm velocity,[8] the elec-
tron density and saturation electron current density are

$$n_e = \frac{1.49 \times 10^{32} \, J_b^{\,2} \, (1-\eta_u) \, \sigma_{ce} \, A}{r_b \, R^2 \, \eta_u \, \sqrt{T_o \, T_e}} \, , \tag{1}$$

$$j_e = \frac{2.62 \times 10^{16} \, J_b \, (1-n_u) \, \sigma_{ce} \, A}{r_b \, R^2 \, n_u \, \sqrt{T_o}} \, , \tag{2}$$

where electron density n_e is in m_1^{-3} electron current density j_e is in A/m_1^2 beam current J_b is in A, charge-exchange cross section σ_{ce} is in m_1^2 atomic weight A is in amu, beam radius r_b is in m, radius from charge-exchange ion source R is in m, neutral and beam electron temperatures T_o and T_e are in °K, and propellant utilization n_u is dimensionless. Substitution of 200.6 for A, $6 \times 10^{-19} \, m^2$ for σ_{ce},[9-11] a typical value of 500°K for T_o, and a typical observation (in this investigation) of 58,000°K (5eV) for T_e, the preceding equations become

$$n_e = 3.3 \times 10^{12} \, J_b^2 \, (1-n_u)/r_b \, R^2 \, n_u, \tag{3}$$

$$j_e = 0.14 \, J_b^2 \, (1-n_u)/r_b \, R^2 \, n_u. \tag{4}$$

It should be noted that lower values of T_e than 5eV have been observed,[12] but the value used here is consistent with the usual small thruster injection voltage of about 20 and the typical ratio of 0.3 for electron temperature divided by injection voltage.[13-14] It should also be noted that electron temperature does not appear in Eq. (2), hence the exact value of this variable should not significantly affect observed values of saturation electron current.

From previous work under this Grant, this isotropic model should be compared to experimental plasma properties normal to the ion beam direction. Rearranging Eq. (4), we obtain

$$n_e \, r_b^3 \, n_u \, / \, J_b^2 \, (1-n_u) = 3.3 \times 10^{12} \, (r_b/R)^2 \tag{5}$$

A curve for this equation is shown in Fig. 8., together with experimental values of the parameter $n_e r_b^3 n_u / J_b^2 (1-n_u)$. The data points shown in Fig. 8., are based upon individual measurements of electron density (not faired values) and range from 86 to 94 degrees relative to the ion beam direction. The data points clearly follow the $1/R^2$ trend of Eg. (5). Further, the 5-cm data obtained during this last Grant support period cover a much wider range of R/r_b than the preceding 15-cm data. From Fig. 8., then, it appears justified to use the $1/R^2$ relationship for spacecraft calculations.

A final point should be made about Fig. 8. concerning the assumed point of origin for the charge-exchange plasma. From the data obtained with the 15-cm thruster, the origin was assumed previously to be one ion beam radius downstream of the accelerator system. A more recent evaluation, which includes the 5-dm data, indicates that one radius of the screen surrounding the thruster would be a better choice than one ion-beam radius. This origin change is only about 4.5 cm for the 15-cm thruster, but results in considerably better agreement between 15-cm and 5-cm data. This redefinition of the origin point is also consistent with results observed using cones downstream of the ion thruster.[4]

Angular Variation of Electron Density

Having justified the inverse-square relationship of electron density with radial distance, it is appropriate to examine the angular variation. The appropriate electron-density parameter can be obtained by rearranging Eq. (3).
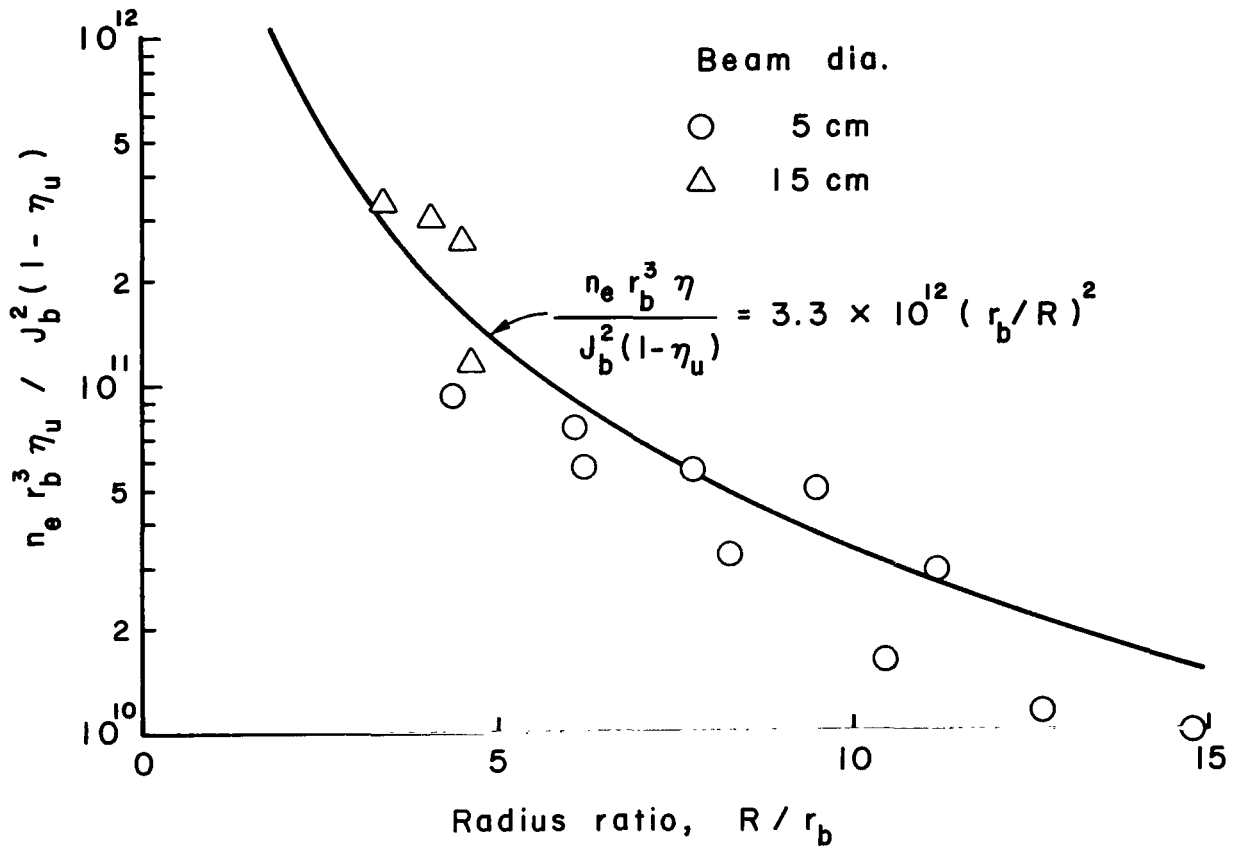
Fig. 8 Effect of radius ratio R/r$_b$ on electron density. The electron density is in a corrected or normalized form to permit inclusion of data from both the 5-cm and 15-cm thrusters. The angle from the beam direction is from 86 to 94 degrees for the data shown.

$$n_e \, r_b \, R^2 \, \eta_u \, / \, J_b(1-\eta_u) \, 3.3 \times 10^{12} \tag{6}$$

The electron density parameter $n_e \, r_b \, R^2 \, \eta_u \, / \, J_b^2 \, (1-\eta_u)$ is plotted against the angle relative to beam direction in Fig. 9. As in Fig. 8, actual electron density measurements were used, not faired values. The point of origin for the charge exchange ions was again assumed to be downstream of the accelerator system by one radius of the screen surrounding the thruster. The average level of the data near 90 degrees is consistent with Eq. (6), as would be expected from Fig. 8. The data for angles less than 30 degrees were omitted because they approached, or were in, the ion-beam volume. Between 30 and 90 degrees the data spread is substantial. This spread was observed earlier and is believed due to the particular beam profiles and angular divergence obtained from the thrusters and operating conditions.[3] The data spread at angles greater than 90 degrees is about equal to that at 90 degrees, indicating that the radial variation at angles greater than 90 degrees would be similar to that shown in Fig. 8. The 15 cm data tend to fall below the 5 cm data at angles greater than 140 degrees, but the total data spread is still believed to approximate the accuracy of the electron density measurements. In view of the larger ranges of experimental variables covered in Fig. 9, the experimental variation with angle shown in Fig. 9 is preferred over the semiemperical equation developed earlier.

Saturation Electron Current Density

For the isotropic model, the saturation electron current density is given by Eq. (4). Rearranging this equation to obtain the electron

Fig. 9 Variation of electron density parameter with
angle from beam direction. Assumed point of
origin is one thruster (ground screen) radius
downstream of the accelerator grid.

current parameter, we obtain

$$j_e \, r_b \, R^2 \, \eta_u \, / \, J_b^2 \, (1-\eta_u) = 0.14 \; , \tag{7}$$

where j_e is the current density (A/m^2) for any surface that is sufficiently positive to collect all the arriving electrons. The most extensive data were obtained in terms of electron density rather than saturation electron current density. To convert from electron density to current density, we use

$$j_e = n_e \, \bar{v}_e \, q \, / \, 4 \; , \tag{8}$$

where $\bar{v}$ is the average electron velocity, $(8kT_e/\pi m_e)^{\frac{1}{2}}$. With the substitution of numerical values, Eq. (8) becomes

$$j_e = 2.49 \times 10^{-15} \, T_e^{\frac{1}{2}} \; . \tag{9}$$

The particular temperature used in this equation needs a word of explanation. The electron temperature in the ion beam has been found to be about twice the electron temperature in the charge exchange region.[3] The 58,000°K (5eV) temperature used to obtain Eq. (3) was measured in the ion beam. The corresponding electron temperature in the surrounding charge-exchange plasma was about 29,000°K (2.5eV). Inasmuch as we are concerned with the charge exchange region, the temperature to use in Eq. (9) should be for that region. That is, about 2.5eV for the 15 cm data and 3.5eV for the 5 cm data. Note that the electron temperature is required because we started with electron density measurements. As shown by Eq. (2), the electron temperature is not a variable in the collection of electron current if the current is measured directly.

Equation (9) was used to convert the electron densities to equivalent electron current densities. The corresponding electron current parameters were plotted in Fig. 10 against the angle from the beam direction. The data distribution in Fig. 10 is similar to that shown for electron density in Fig. 9. At angles less than 90 degrees from the beam direction the data spread is large due to the influence of the particular beam profile. At angles of 90 degrees, or more, the data spread approximates the accuracy uncertainty of Langmuir probe measurements.

Planar Probe Measurements

The electron current densities of Fig. 10 were obtained from electron densities and electron temperatures, both of which were obtained from Langmuir probes. Because the probe diameter was small compared to the Debye length, there was no direct measurement of the saturation electron density. The planar probe was designed to make such a direct measurement. The Debye length in the vicinity of the planar probe was 2-3 cm. The 5 cm guard around the probe was therefore sufficient to eliminate edge effects around the central 10 cm square probe surface (see Fig. 4). The potential of the planar probe was 15 to 25 V above the local plasma potential, which was determined from Langmuir probe survey. The potential should therefore have been sufficiently positive to assure collection of all arriving electrons.

The current collected by the planar probe was 0.22 mA. For the radial location used, together with thruster operating conditions, this current corresponded to an electron current parameter of 0.050.
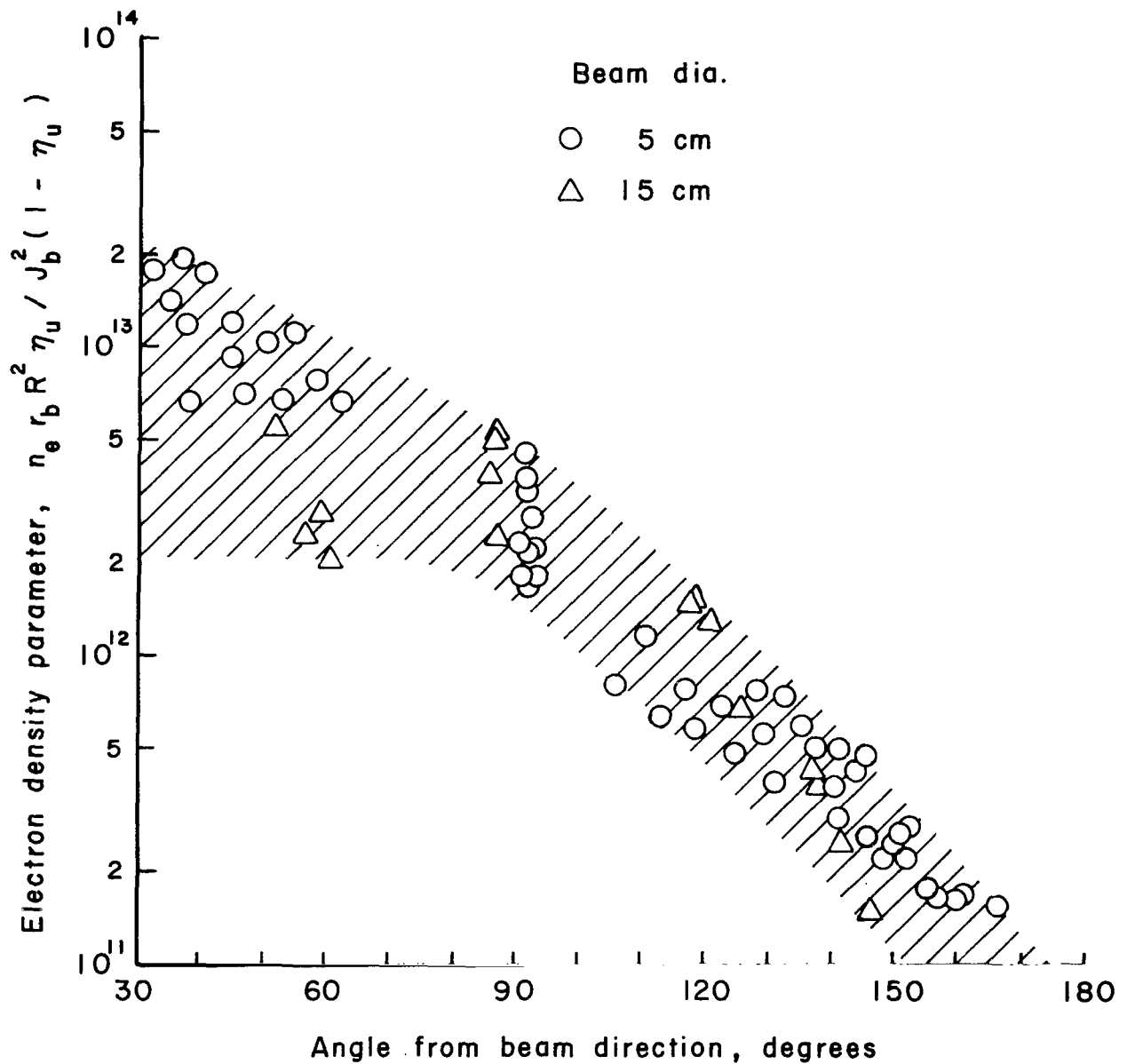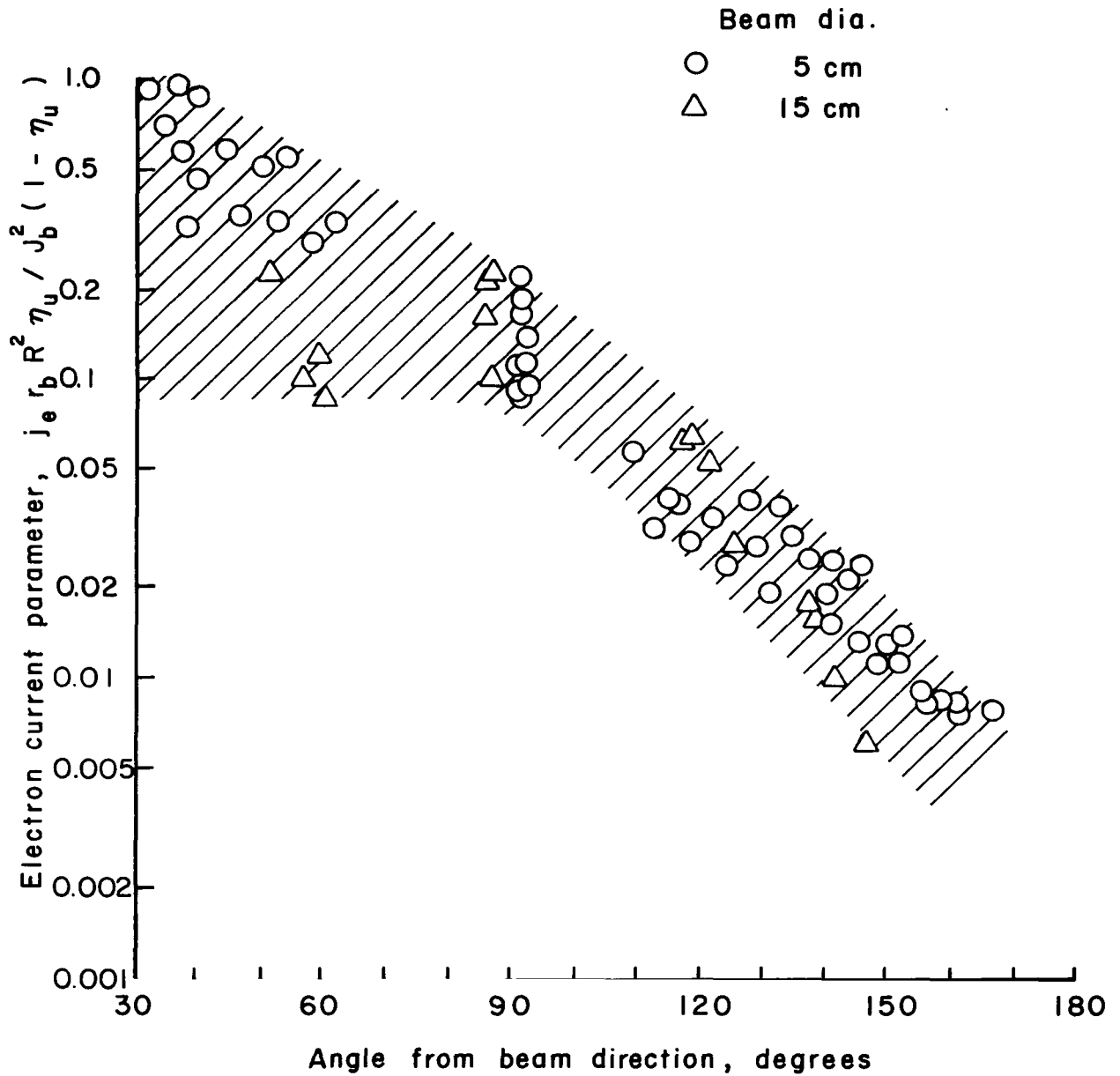
Fig. 10 Variation of electric current (density)
parameter with angle from beam direction.
Assumed point of origin is one thruster
(ground screen) radius downstream of
accelerator grid.

This value, at an angle of 122 degrees from the beam direction, is near the center of the data spread in Fig. 10. The planar probe measurement thus constitutes a separate and independent check on the calculated current densities used in Fig. 10.

Pin-Hole Probe Measurements

The major objective of the overall investigation was to evaluate the charge-exchange plasma surrounding an electric thruster. As such, the pin-hole probe was considered a minor experiment that could be added with only a small increase in the total experimental effort, inasmuch as the charge-exchange plasma was already available.

The electron density in the vicinity of the plasma probe was about 9×10^{10} m^{-3}. This density, together with the 3.5eV electron temperature, resulted in a Debye length of about 5 cm. Comparing this length to the probe geometries investigated, the plain probe (Fig. 4 (a)) was larger than the Debye length, the coarse mesh (Fig. 4 (b)) was roughly equal to the Debye length, and the fine mesh was smaller than the Debye length. The purpose of the mesh was, of course, to interrupt either surface conduction or plasma-sheath focusing, thereby reducing the current collected by the pin hole.

The current-collection data for the pin-hole probe are shown in Fig. 11. The current at a given collection voltage shows a systematic decrease from the plain probe to the coarse mesh to the fine mesh. The magnitude of the decrease, though, is much smaller than the area reduction from the total probe to the area enclosed by one mesh square. A shortcoming of the data shown in Fig. 11 is that collection voltages
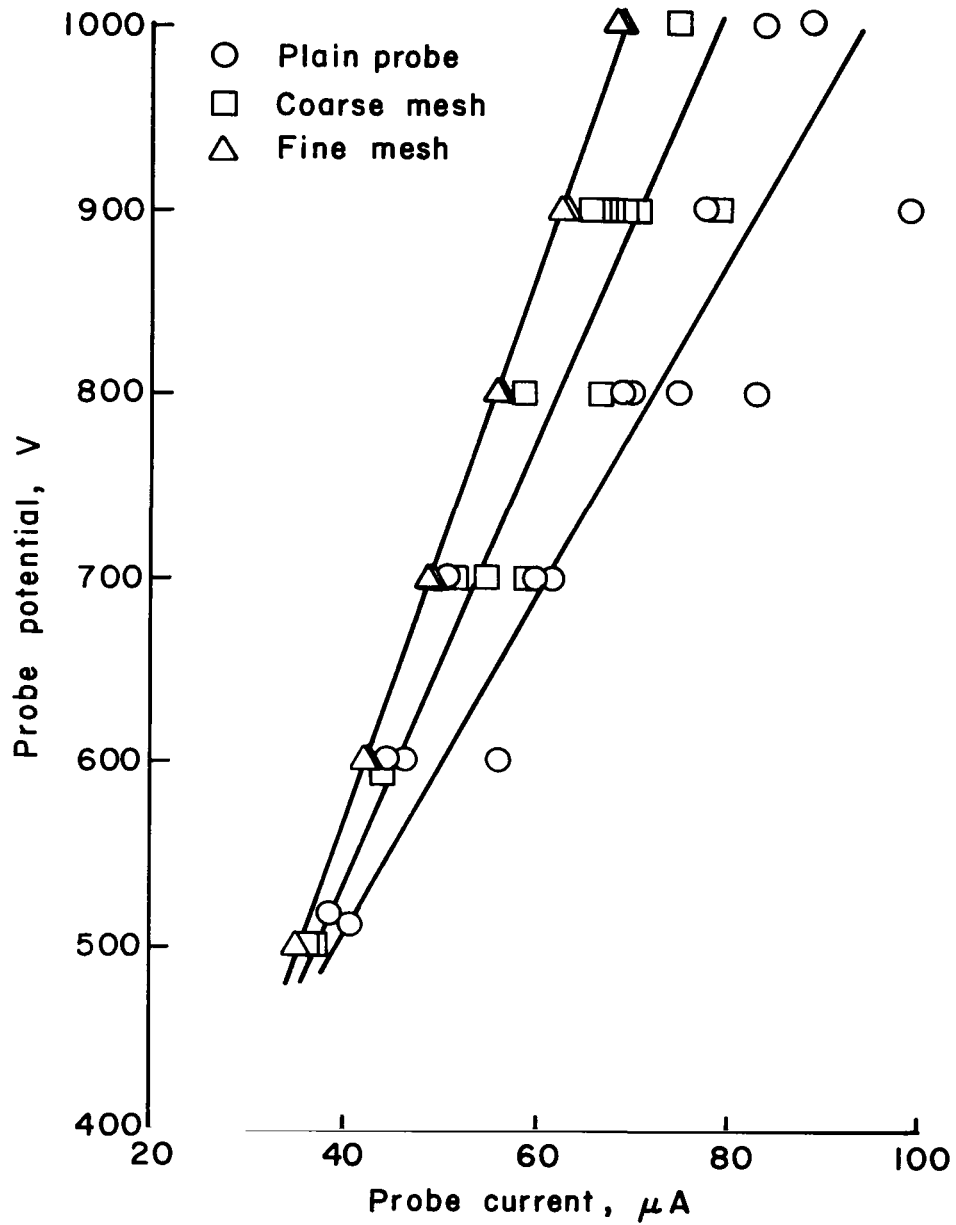
Fig. 11 Current collected by pin-hole probe.
(See Fig. 5 for probe configruations.)

were not high enough to encounter the sharp increase in collection current that is normally found. The effect of insulator area is usually larger above this increase, so that the three configurations of Fig. 11 might be expected to diverge more at higher voltages.

CALCULATION PROCEDURE

The assumed point of origin for the charge-exchange plasma surrounding a thruster is indicated in Fig. 12. For a single thruster this point is one thruster radius r_t downstream of the accelerator grid and on the thruster centerline, as shown in Fig. 12(a). For a circular array of thrusters (Fig. 12(b)), the effective point of origin would be expected (from conical collector tests[4]) to be one radius of the thruster array r_t' downstream of the array center. For a noncircular array, the effective array radius r_t' would be expected to be between the maximum and minimum values from the center of the array. A noncircular array would probably also cause some departures from axial symmetry. But the magnitude of these departures cannot be estimated at the present time, except that the charge-exchange plasma would probably depart less from axial symmetry than the array.

The charge-exchange plasma at some point of interest (see Fig. 12(a)) is a function of the radial distance from the assumed point of origin, R, and the angle relative to the beam direction, θ, in addition to the thruster parameters of beam radius r_b, beam current J_b, and thruster propellant utilization η_u. As shown by Figs. 9 and 10, the electron density n_e and saturation electron current density* j_e are effectively correlated by parameters including these variables. Rather than use

---

* This current density is the value that would be obtained at any surface that is sufficiently positive to collect all electrons approaching it and sufficiently large to make edge effects negligible.
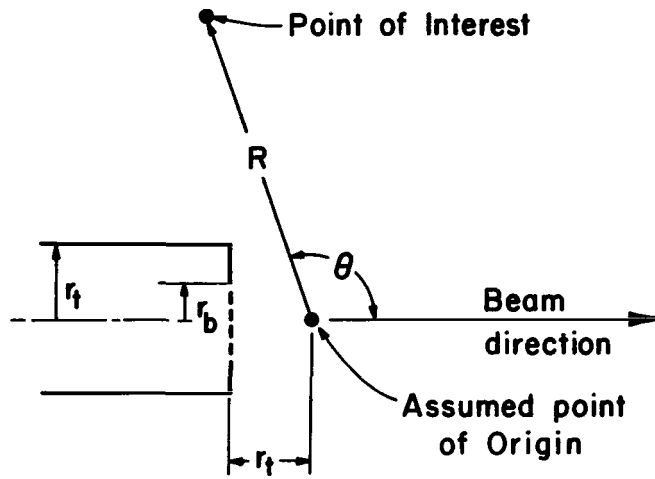
(a) Single thruster
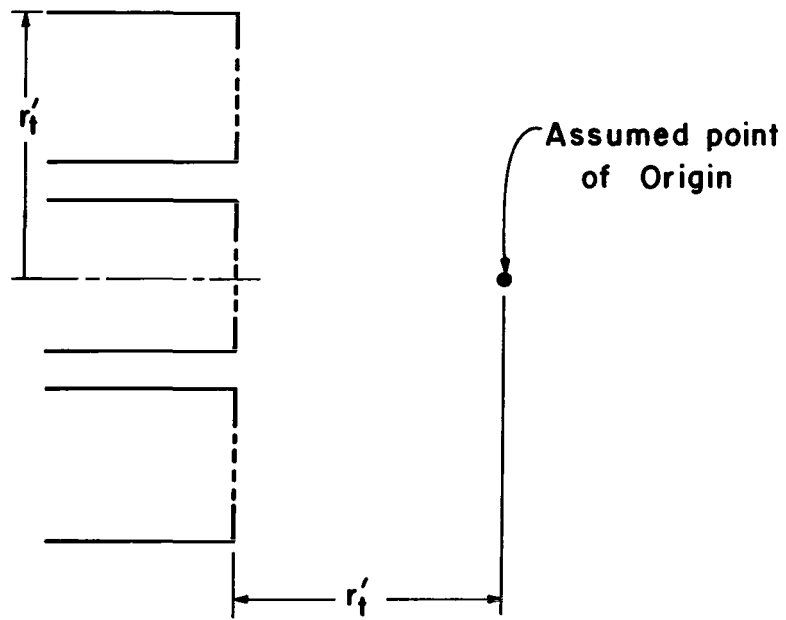
(b) Thruster array

Fig. 12 Parameters for calculation of
charge-exchange plasma around thruster.

Figures 9 and 10 for calculations, the upper envelopes of the data distributions in these figures are tabulated in Tables I and II as functions of the angle θ. To calculate the electron density and saturation electron current density, select values from Tables I and II for the angle θ of interest and substitute in the equations below:

$$n_e = [J_b^2 (1-\eta_u) / r_b R^2 \eta_u][\text{Table I Param}] \, m^{-3} \tag{10}$$

$$j_e = [J_b^2 (1-\eta_u) / r_b R^2 \eta_u][\text{Table II Param}] \, A/m^2 \tag{11}$$

The beam current J_b is in A, the propellant utilization η_u is dimensionless, and both the beam radius r_b and the radius R are in m.

Table I - Electron density parameter as a function of
angle from beam direction. (From Fig. 9.)

θ, deg.	Param.	θ, deg.	Param.	θ, deg.	Param.
30	2.3×10^{13}	80	6.6×10^{12}	130	1.0×10^{12}
40	1.8×10^{13}	90	5.0×10^{12}	140	6.2×10^{11}
50	1.4×10^{13}	100	3.5×10^{12}	150	3.7×10^{11}
60	1.1×10^{13}	110	2.4×10^{12}	160	2.2×10^{11}
70	8.6×10^{12}	120	1.6×10^{12}	170	1.3×10^{11}

Table II - Electron current density parameter as a
function of angle from beam direction. (From Fig. 10.)

θ, deg.	Param.	θ, deg.	Param.	θ, deg.	Param.
30	1.2	80	0.32	130	0.052
40	0.94	90	0.23	140	0.032
50	0.72	100	0.17	150	0.019
60	0.55	110	0.12	160	0.011
70	0.42	120	0.082	170	0.064

Sample Calculation

The electron density and saturation electron current density have been calculated for an 8-cm thruster as a sample calculation. The operating conditions selected were obtained from literature[15, 16] and are:

Total neutral flow, 0.0914 A-equivalent

Net accelerating potential difference, 1205. V

Beam current, J_b, 0.072 A

Propellant utilization, η_u, 0.79

The pertinent physical dimensions are:

Radius ion beam, r_b, 0.04 m

Radius of ground screen, 0.084 m

The operating conditions given assume the use of a small hole accelerator grid, which permits higher propellant utilization than would otherwise be practical.

The point of interest for these calculations was arbitrarily assumed to be 1.0 m radially out from the thruster centerline and 0.5 m upstream of the accelerator grid. The assumed point of origin for the charge-exchange plasma is one ground-screen radius downstream of the accelerator grid (see Fig. 12(a)). This gives a radius R of

$$R = (1.0^2 + 0.584^2)^{1/2} = 1.16 \text{ m.}$$

For the point of interest selected, the angle relative to the beam direction is

$$\theta = 90 + \text{arc tan} (0.584 / 1.0)$$

$$= 120°.$$

From Table I, the electron density parameter for 120 degrees is 1.6×10^{12}. (Interpolation could have been used for an angle between those given in the table.) Substitution of the numerical values for the various parameters in Eq.(10) yields an electron density of

$$n_e = [0.072^2(1-0.79) / 0.04 \times 1.16^2 \times 0.79][1.6 \times 10^{12}]$$
$$= 4.1 \times 10^{10} \ m^{-3}.$$

From Table II, the electron current density parameter for 120 degrees is 0.083. Substitution in Eq. (11) then yields a saturation electron current density of

$$j_e = [0.072^2(1-0.79) / 0.04 \times 1.16^2 \times 0.79][0.082]$$
$$= 0.0021 \ A/m^2.$$

This current density is, of course, the value that would be collected by any surface that was sufficiently positive to collect all electrons directed toward that surface. It is also assumed that the surface in question is approximately normal to the radius R.

The calculated values for n_e and j_e represent the upper edge of the distributions shown in Figs. 9 and 10, hence should be conservative (high) values. From the distributions shown near the angle of 121 degrees, the actual values may be as much as a factor of 3 lower.

The foregoing is true for electron temperatures close to those observed in the experimental investigation. For the current density j_e, the result should be unaffected by changes in electron temperature. This is because Eq. (11) is based on Eq. (2), which has no electron temperature in it.

For the electron density n_e, an effect of electron temperature would be expected. As shown by Eq. (1), upon which Eq.(10) is based, the electron density should vary inversely as the square root of electron temperature. The measurements of this investigation indicated 2.5 and 3.5 eV for the 15-cm and 5-cm thrusters, respectively. The electron temperature within a 30-cm thruster beam was found to be 0.35 eV.[12] Including the observation in this investigation that beam electron temperature is about twice the electron temperature in the surrounding charge-exchange region, there is an uncertainty in electron temperature of up to a factor of 20. This temperature uncertainty translates into a factor of 4 or 5 in electron density uncertainty. Specifically, n_e could be 4 or 5 times as high as the calculated value due to a lower electron temperature.

Although the total electron density uncertainty due to electron temperature must be of the order of this factor of 4 or 5, the probable uncertainty in electron density is believed to be smaller. The observed electron temperature appears to decrease with increasing thruster size. Such a trend has also been observed elsewhere.[17] A similiar decrease in Maxwellian electron temperature has also been observed within the discharge chamber for increasing thruster size.[18] Inasmuch as the 8-cm thruster size in the sample problem is between the 5-cm and 15-cm sizes used in this investigation, the electron temperature might be expected to also be intermediate. Conversely, if a calculation were being made for a 30-cm thruster, a more serious consideration should probably be given to the effect of a lower electron temperature.

The sample calculation presented above is for a single isolated thruster. An array of thrusters will produce a total charge-exchange plasma that is greater than the sum of that produced by the same number of isolated thrusters. This is because the beam of each thruster passes through the neutral efflux of all the thrusters, thus increasing the charge-exchange ion production over the value that would be obtained from an isolated thruster. Including this interaction requires tedious, but straightforward free-molecular-flow calculations. Some simplification of these calculations is possible by asssuming that the beam from each thruster is concentrated near the axis of that thruster.

CONCLUDING REMARKS

The validity of simulating the charge-exchange plasma generated by a thruster in space was investigated by varying the mercury background pressure in the vacuum chamber. The resulting measurements indicate that most of the charge-exchange plasma found in the vacuum chamber would also be present in space.

The survey of the charge-exchange plasma surrounding a 5-cm thruster gave results generally in agreement with earlier surveys using a 15-cm thruster.

The variation of electron density was investigated over a wide range of radial distance relative to the beam radius. The data for this extended range agreed closely with the inverse-square theoretical model, and should justify the calculations at even larger radial distances for spacecraft environments.

The angular variation of electron density and saturation electron current density in the charge-exchange plasma was found to follow a slightly different trend than the semiemperical equation obtained earlier. Plots of the experimental data appear to be the best basis for predicting angular variations of these plasma parameters. These plots include data sets from both the 5-cm and 15-cm thrusters, with excellent agreement between the two sets.

Electron temperature is a variable that will affect the electron density, but not the saturation electron current density. Because the effect is through the square-root temperature, the estimates of electron density should still be useful.

The experimental results are also presented in tabular form to aid calculation. A calculation procedure is included, together with a sample calculation of electron density and saturation electron current density.

REFERENCES

1. R. Worlock, G. Trump, J. M. Sellen, Jr., and R. F. Kemp, _AIAA Paper_ No. 73-1101 (1973).

2. W. Knauer, J. R. Bayless, G. T. Todd, and J. W. Ward, _NASA Contractor Report CR-72675_, May 1970.

3. H. R. Kaufman, _NASA Contractor Report_ CR-134844, June 1975.

4. H. R. Kaufman, _NASA Contractor Report_ CR-135099, October 1976.

6. G. Isaacson, in _NASA Contractor Report_ CR-134755 (by P. J. Wilbur), Appendix B, December 1974.

7. F. F. Chen, "Plasma _Diagnostic Techniques_" (Huddlestone and Leonard, Eds.), Chap. 4, Academic Press, N.Y. 1965.

8. D. Bohm, _in_ "The Characteristics of Electrical Discharges in Magnetic Fields," (A. Guthrie and R. K. Wakerling, Eds.), pp. 77-86, McGraw-Hill Book Co., 1949.

9. R. M. Kushnir, B. M. Palyukh, and L. A. Sena, _Bull. Acad. Sci. USSR, Phys. Ser._, Vol. 23, pp. 995-999 (1959).

10. I. P. Iovitsu and N. Ionescu-Pallas, Sov. _Phys. - Tech. Phys._, Vol. 4, pp. 781-791 (1960).

11. D. Zuccaro, NASA _Contractor Report_ CR-72398 (1968).

12. G. K. Komatsu, R. K. Cole, D. K. Hoffmaster, and J. M. Sellen, Jr., _AIAA Paper_ No. 75-428 (1975).

13. H. S. Ogawa, R. K. Cole, and J. M. Sellen, Jr., _AIAA Paper_ No. 69-263 (1969).

14. H. S. Ogawa, R. K. Cole, and J. M. Sellen, Jr., _AIAA Paper_ No. 70-1142 (1970).

15. B. A. Banks, et al., _AIAA Paper_ No. 74-1116 (1974).

16. S. Nakanishi, _AIAA Paper_ No. 76-1022 (1976).

17. J. M. Sellen, Jr., Personal communication, Dec. 1977.

18. P. J. Wilbur, Personal communication, Dec. 1977.

DISTRIBUTION LIST

National Aeronautics and Space Administration
Washington, D. C.   20546
Attn: RPE/Mr. Wayne Hudson   1
       Mr. Daniel H. Herman, Code SL   1

National Aeronautics and Space Administration
Lewis Research Center
21000 Brookpark Road
Cleveland, Ohio   44135
Attn: Research Support Procurement Section
       Mr. Allen Jones, MS 500-313   1
       Technology Utilization Office, MS 3-19   1
       Report Control Office, MS 5-5   1
       Library, MS 60-3   2
       N. T. Musial, MS 600-113   1
       Spacecraft Technology Division, MS 501-8
          Mr. H. Douglass   1
          Mr. R. Finke   1
          Mr. D. Byers   1
          Mr. B. Banks   1
          Mr. S. Domitz   1
          Mr. F. Terdan   1
          Mr. W. Kerslake   1
          Mr. Vincent K. Rawlin   20
          Mr. M. Mirtich   1
       Physical Science Division, MS 301-1
          Mr. W. E. Moeckel   1

National Aeronautics and Space Administration
Marshall Space Flight Center
Huntsville, Alabama   35812
Attn: Mr. Jerry P. Hethcoate   1

Research and Technology Division
Wright-Patterson AFB, Ohio   45433
Attn: (ADTN) Lt. David A. Fromme   1

NASA Scientific and Technical Information Facility
P. O. Box 8757
Baltimore/Washington International Airport
Baltimore, Maryland   21240   40

Case Western Reserve University
10900 Euclid Avenue
Cleveland, Ohio   44106
Attn: Dr. Eli Reshotko   1

Royal Aircraft Establishment
Space Department
Farnborough, Hants, England
Attn: Dr. D. G. Fearn   1

United Kingdom Atomic Energy Authority
Culham Laboratory
Abingdom, Berkshire, England
Attn: Dr. P. J. Harbour   1
       Dr. M. F. A. Harrison   1
       Dr. T. S. Green   1

National Aeronautics and Space Administration
Goddard Space Flight Center
Greenbelt, Maryland 20771
Attn: Mr. W. Isley, Code 734   1
       Mr. R. Bartlett, Code 713   1
       Mr. R. Callens, Code 734   1

SAMSO
Air Force Unit Post Office
Los Angeles, California 90045
Attn: Capt. D. Egan/SYAX   1

Comsat Laboratories
P. O. Box 115
Clarksburg, Maryland 20734
Attn: Mr. B. Free   1
       Mr. O. Revesz   1

Rocket Propulsion Laboratory
Edwards AFB, California 93523
Attn: LKDA/Mr. Tom Waddell   2

DFVLR - Institut für Plasmadynamik
Technische Universitat Stuttgart
7 Stuttgart-Vaihingen
Allmandstr 124
West Germany
Attn: Dr. G. Krülle   1
       Mr. H. Bessling   1

Giessen University
1st Institute of Physics
Giessen, West Germany
Attn: Professor H. W. Loeb   1

Jet Propulsion Laboratory
4800 Oak Grove Drive
Pasadena, California 91102
Attn: Dr. Kenneth Atkins   1
       Technical Library   1
       Mr. Eugene Pawlik   1
       Mr. James Graf   1

Electro-Optical Systems, Inc.
300 North Halstead
Pasadena, California 91107
Attn: Mr. R. Worlock   1
       Mr. E. James   1
       Mr. W. Ramsey   1

```
TRW, Inc.
TRW Systems
One Space Park
Redondo Beach, California  90278
Attn:  Mr. M. Huberman                                              1
       Dr. J. M. Sellen                                            1
       Dr. S. Zafran                                               1

National Aeronautics and Space Administration
Ames Research Center
Moffett Field, California  94035
Attn:  Technical Library                                           1

National Aeronautics and Space Administration
Langley Research Center
Langley Field Station
Hampton, Virginia  23365
Attn:  Technical Library                                           1

Hughes Research Laboratories
3011 Malibu Canyon Road
Malibu, California  90265
Attn:  Dr. Jay Hyman                                               1
       Mr. J. H. Molitor                                           1
       Dr. R. L. Poeschel                                          1
       Mr. R. Vahrenkamp                                           1
       Dr. John R. Beattie                                         1

United States Air Force
Office of Scientific Research
Washington, D. C.  20025
Attn:  Mr. M. Slawsky                                              1

Princeton University
Princeton, New Jersey  08540
Attn:  Mr. W. F. Von Jaskowsky                                     1
       Dean R. G. Jahn                                             1
       Dr. K. E. Clark                                             1

Communications Research Centre
Ottawa, Ontario, Canada
Attn:  Dr. W. F. Payne                                             1

Joint Institute for Laboratory Astrophysics
University of Colorado
Boulder, Colorado  80302
Attn:  Dr. Gordon H. Dunn                                          1

Department of Aeronautics and Astronautics
Stanford University
Stanford, California  94305
Attn:  Professor Howard S. Seifert                                 1
```

Boeing Aerospace Company
P. O. Box 3999
Seattle, Washington 98124
Attn: Mr. Donald Grim   1

Intelcom Rad Tech
7650 Convoy Court
P. O. Box 80817
San Diego, California 92138
Attn: Dr. David Vroom   1

Lockheed Missiles and Space Company
Sunnyvale, California 94088
Attn: Dr. William L. Owens
       Propulsion Systems, Dept. 62-13   1

Fairchild Republic Company
Farmingdale, New York 11735
Attn: Dr. William Guman   1

COMSAT Corporation
950 L'Enfant Plaza SW
Washington, D. C. 20024
Attn: Mr. Sidney O. Metzger   1

Electrotechnical Laboratory
Tahashi Branch
5-4-1 Mukodai-Machi, Tanashi-Shi
Tokyo, Japan
Attn: Dr. Katsuva Nakayama   1

Office of Assistant for Study Support
Kirtland Air Force Base
Albuquerque, New Mexico 87117
Attn: Dr. Calvin W. Thomas OAS Ge   1
       Dr. Berhart Eber OAS Ge   1

Bell Laboratories
600 Mountain Avenue
Murray Hill, New Jersey 07974
Attn: Dr. Edward G. Spencer   1
       Dr. Paul H. Schmidt   1

Massachusetts Institute of Technology
Lincoln Laboratory
P. O. Box 73
Lexington, Massachusetts 02173
Attn: Dr. H. I. Smith   1

Sandia Laboratories
Mail Code 5742
Albuquerque, N.M. 87115
Attn: Mr. Ralph R. Peters   1

Service du Confinement des Plasma
Centre d'Etudes Nucléaires - F.A.R.
B.P. 6
92260 Fontenay-aux-Roses
France
Attn: Dr. J. F. Bonal   1